Polyelectrolyte brush bilayers in weak interpenetration regime: Scaling theory and molecular dynamics simulations

Parth Rakesh Desai, Shayandev Sinha, and Siddhartha Das
Department of Mechanical Engineering, University of Maryland, College Park, Maryland 20742, USA

(Received 18 August 2017; published 13 March 2018)

We employ molecular dynamics (MD) simulations and develop scaling theories to quantify the equilibrium behavior of polyelectrolyte (PE) brush bilayers (BBLs) in the weakly interpenetrated regime, which is characterized by $d_0 < d_g < 2d_0$, where d_g is the gap between the opposing plates where the PE brushes are grafted and d_0 is the unperturbed height of a PE brush grafted at a single plate. Scaling predictions establish that, for the weakly interpenetrated osmotic PE BBLs $\delta \sim N^{1/2}(2 - d_g/d_0)^{1/2}$ (where δ is the interpenetration length and N is the number of Kuhn segments in PE brush). MD simulations excellently recover this dependence of δ on N and the extent of interpenetration (quantified by d_g/d_0). These predictions, unlike the existing studies, establish a finite interpenetration for all values of d_g/d_0 as long as $d_g < 2d_0$. Finally, we quantify the monomer and counterion concentration distributions and point out that these two distributions may quantitatively deviate from each other at locations very close to the channel centerline, where the interpenetration-induced monomer concentration can be significantly low.

DOI: 10.1103/PhysRevE.97.032503

I. INTRODUCTION

Decorating solid-liquid interfaces by grafting them with polymer and polyelectrolyte (PE) brushes has seen massive applications in a myriad of disciplines ranging from nanoscale transport and sensing to drug delivery and oil recovery [1–14]. In the brush-like configuration, the polymer and PE molecules extend vertically away from the grafting surface attaining a height d_0 that is larger than the radius of gyration of the polymer-PE molecule. The major focus has been studying the behavior of these brushes grafted to a single solid-liquid interface [15–21]. Intermolecular and intramolecular electrostatic repulsions ensure a swelling of the PE brushes grafted to a single interface—concentration of counterions and added salt ions dictate the extent of this swelling [22–29]. An important variant of the brush problem is the problem of polymer-PE brush bilayers (BBLs), where the polymer-PE brushes are grafted to two opposing surfaces having a separation of d_g, such that $d_g < 2d_0$ [30] (here d_0 is the unperturbed brush height). The main interest in studying the polymer-PE BBLs is the large lubricity witnessed in this regime [31], embracing applications associated with friction reduction [31–39], development of lubricating coatings [40], and fabrication of artificial hip and knee joints [41,42].

Domains of interest for polymer-PE BBLs are either (a) the weak interpenetration (IP) regime ($d_0 < d_g < 2d_0$) or (b) the intermediate IP regime (where $d_g < d_0$, i.e., there is a physical compression) [30]. Theoretical [18,43–57], numerical [35–39,43–47,47–51,58–63], and experimental [32–34,64–69] investigations have primarily probed the intermediate IP regime because the BBL behavior in this regime is best suited to understand the brush-induced lubrication behavior of human joints, thereby motivating the development of artificial hip and knee joints. Kreer in a recent review article wonderfully summarizes the findings of several of these papers [30]. On the other hand, in a recent paper we employed molecular dynamics (MD) simulations and scaling theory to elucidate the behavior of polymer BBLs in the *weak IP regime*—we report distinctly different interpenetration and compressive behavior as compared with those for the intermediate IP regime [70]. Unlike the polymer BBLs, as has been pointed out by Kreer [30], much less is known about the PE BBLs. A relevant theoretical study on the topic is by Zhulina and Rubinstein [71], who developed scaling laws to pinpoint the configuration of PE BBLs and the resulting lubrication behavior under different conditions of IP. However, in this theoretical model [71], as well as in other similar theoretical models on PE BBLs, the focus has been primarily on intermediate and strong IP domains and the analyses mostly neglect the excluded volume interactions [71–73]. The neglect of the excluded volume interactions becomes problematic either for very weak Bjerrum length ℓ_B [i.e., $\ell_B \to 0$, where $\ell_B = e^2/(\epsilon_0\epsilon_r k_B T)$, e is the electronic charge, $k_B T$ is the thermal energy, ϵ_0 is the permittivity of free space, and ϵ_r is the relative permittivity of the vacuum] representing quasineutral brushes or for highly charged brushes (i.e., where $\ell_B > \ell_B^{\text{crit}}$) [74]. Another important related study is by Kumar and Seidel [75], who carried out MD simulations to probe the interaction of the PE BBLs under different extent of IP—however, their analysis could only provide a "phenomenological" scaling match (and not a free-energy-derived scaling match) to the MD simulation results for the IP length. Analyses have also been conducted to quantify the compressive force for the PE BBLs in the intermediate IP regime—the results demonstrate a relatively acceptable match of scaling calculation results with the experimental data for large salt concentration, while for weak salt concentration the match is completely off [76]. On the other hand, one witnesses distinct deviation between the theoretical [72] and MD simulation [74,77] prediction of the compressive forces for the PE BBLs. Furthermore, theoretical

calculations, MD simulations, and experiments have been carried out to quantify the shear forces for the PE BBLs in the intermediate IP regime—issues that have been considered are linear and nonlinear responses to small and large applied shear (quantified in terms of the corresponding Weissenberg number) and the resultant shear force, kinetic friction coefficient, and the shear viscosity and their dependence on ℓ_B [67,74,77,78].

The aim of this present paper is to provide the first complete quantitative understanding of the PE BBLs in the weak IP regime. For this purpose, we conduct extensive MD simulations and develop a scaling theory. Our theory establishes that, for the weakly interpenetrating osmotic PE BBLs, the interpenetration length δ [44] is expressed as $\delta \sim N^{1/2}(2 - d_g/d_0)^{1/2}$. Our MD simulation results match excellently with this scaling prediction, elucidating this dependence of δ on N and the degree of IP (d_g/d_0). Our analysis, therefore, establishes that a finite δ is possible for all values of d_g/d_0 in the weak IP regime (i.e., $d_0 < d_g < 2d_0$). This is the central finding of this paper. This result contradicts the analysis of the existing studies on PE BBLs in weakly interpenetrated regime [71,75]—these studies suggest that in the weak IP regime, the interpenetration may not be at all possible [71] or possible only if d_g is very close to d_0 [75]. While Zhulina and Rubinstein [71] did not carry out any MD simulation to validate their scaling result, Kumar and Seidel [75] merely used a "phenomenological" theory (without any rigorous free-energy basis) to match their MD results. On the other hand, in this paper, we conduct MD simulations and match the results with a scaling theory that has been rigorously derived from free-energy considerations. Second, we obtain the distribution of the monomer and the counterion concentrations. We consider a grafting density that is large enough to ensure that the brushes are osmotic brushes. Therefore, one would expect that the counterions would remain tightly bound to the PE brushes, enforcing a very similar monomer and counterion concentration distributions across the channel. While such similarities are indeed witnessed for the majority of locations across the channel, at locations very close to the channel centerline one may witness a quantitative deviation between the counterion and monomer distribution. We anticipate that our detailed analysis involving MD simulations and rigorous free-energy-based scaling calculations will provide an important fundamental basis for quantifying the properties of PE BBLs of specified degree of interpenetration.

II. SCALING LAWS

The purpose of this section is to derive the scaling laws for the weakly interpenetrated PE BBLs. The calculations will require knowledge of the scaling laws for a single PE chain as well as a single noninterpenetrated PE brush under different conditions of the PE charge. These results are well known in the literature [22,71]. We briefly review them here in Secs. II A–II C for the sake of continuity.

A. Scaling laws for a single polyelectrolyte chain

Here we first revisit the scaling expression for a single PE chain in a salt-free solution. The energy of the chain (F) is a sum of the elastic energy $F_{\rm els}$ and the electrostatic energy $F_{\rm elec}$ [71]:

$$F = F_{\rm els} + F_{\rm elec}, \tag{1}$$

where

$$F_{\rm els} \approx k_B T \left(\frac{L_e}{aN^{\nu}}\right)^{\frac{1}{1-\nu}}, \tag{2}$$

$$F_{\rm elec} \approx k_B T \ell_B \frac{(fN)^2}{L_e}. \tag{3}$$

In the above equations, L_e is the end-to-end distance of the PE chain, $k_B T$ is the thermal energy, $\ell_B = e^2/(\epsilon_0 \epsilon_r k_B T)$ is the Bjerrum length, N is the total number of Kuhn segments of length a in the PE chain, f is the fraction of charged Kuhn segments, and ν is the exponent, which is approximately equal to 3/5 for a good solvent.

The equilibrium value of L_e is obtained by minimizing Eq. (1) with respect to L_e, yielding:

$$L_e \sim aN(uf^2)^{\frac{1-\nu}{2-\nu}}, \tag{4}$$

where

$$u = \frac{\ell_B}{a} = \frac{e^2}{a\epsilon_0\epsilon_r k_B T}. \tag{5}$$

A single PE chain can be visualized as a string of N/g_e number of blobs, where g_e is the number of Kuhn segments in each blob. Inside each blob, the PE chain segment takes the conformation of the parent PE chain. Therefore, the end-to-end distance for this blob-encased PE segment (this end-to-end distance is also the diameter of the blob) is

$$\xi_e \sim a g_e (uf^2)^{\frac{1-\nu}{2-\nu}}. \tag{6}$$

On the other hand, the local chain statistics (important for length scales smaller than ξ_e) leads to [71]

$$\xi_e \sim a g_e^{\nu}. \tag{7}$$

Using Eqs. (6) and (7), we eventually obtain [71]

$$\xi_e \sim a(uf^2)^{-\frac{\nu}{2-\nu}}, \tag{8}$$

$$g_e \sim (uf^2)^{-\frac{1}{2-\nu}}. \tag{9}$$

We can also express ξ_e in terms of the monomer concentration c (having units of $1/\mathrm{m}^3$) within each blob, where

$$c \sim \frac{g_e}{\xi_e^3}. \tag{10}$$

Using Eq. (10) to replace g_e in Eq. (8), we eventually obtain

$$\xi_e \sim (ac)^{-1/2}(uf^2)^{-\frac{1-\nu}{4-2\nu}}. \tag{11}$$

B. Scaling laws for a single polyelectrolyte brush

We consider a grafting density σ_g of the grafted PE system such that $\sigma_g > \sigma_g^*$ [where $\sigma_g^* \sim 1/L_e^2$, with Eq. (4) expressing L_e]. Under this condition, the grafted PE molecules will form brushes. However, the nature of these brushes (and accordingly the brush height) will be dictated by the precise value of the grafting density σ_g. In case, the $\sigma_g^* < \sigma_g < \sigma_{\rm osm}$, the grafted PE molecules will form *Pincus brushes*, while if $\sigma_g > \sigma_{\rm osm}$ the grafted PE molecules will form *osmotic brushes* [22,71]. Here

σ_{osm} is the critical grafting density that dictates the crossover between the Pincus and the osmotic brush regimes and can be expressed as [71]

$$\sigma_{osm} \sim \frac{1}{\ell_B a N^2 f^{2-\nu}}. \tag{12}$$

For the PE brushes in the Pincus regime, the brush height is dictated by the balance of the electrostatic and the elastic energy of the PE brushes yielding an equilibrium brush height of Ref. [71]:

$$d_{0,PB} \sim a(uf^2\sigma_g a^2)^{\frac{1-\nu}{\nu}} N^{\frac{2-\nu}{\nu}}. \tag{13}$$

On the other hand, for the osmotic brushes, the grafting density is large enough to ensure that the counterions become strongly localized, thereby governing the brush properties. Therefore, for this case, the brush height is determined by the balance of the osmotic pressure of the counterions and the elastic energy of the brushes, yielding [22,71]

$$d_{0,OB} \sim aNf^{1-\nu}. \tag{14}$$

For the osmotic brushes, the counterions are strongly bound to the PE brushes, with the counterion layer thickness d_{CI} being [79]

$$d_{CI} \sim d_{0,OB} + \tfrac{3}{2}\ell_{GC}. \tag{15}$$

Here $\ell_{GC} = \frac{1}{2\pi\ell_B N f\sigma}$ is the Gouy–Chapman length, which is of the order of few angstroms for a fully charged brush ensuring $d_{CI} \approx d_{0,OB}$.

C. Scaling laws for polyelectrolyte brush bilayers in intermediate interpenetration regime

The intermediate IP regime is characterized by $d_g < d_0$, where depending on the grafting density, either Eq. (13) or Eq. (14) will define d_0.

For the PE brushes, very much like the polymer brushes, the monomer-monomer interaction can be described by a classical parabolic molecular interaction field. This leads to an IP length δ as [45,70]

$$\delta \sim a^{4/3} N^{2/3} d_g^{-1/3}. \tag{16}$$

Equation (16) is also the expression for the height of the polymer brushes (in the molten state) in the intermediate IP regime. Such identical expression [Eq. (16)] for the IP length for both the polymer and the PE brushes in the intermediate IP regime has already been confirmed by the existing literature [71].

Equation (16) is a valid scaling law for the molten PE brushes. For semidilute brushes, we consider that the brushes are divided into blob-like compartments. Consequently, similar to previous studies [45,70,71], one should replace a by ξ_e [see Eq. (11) for the expression of ξ_e] and N by N/g_e [see Eq. (9) for the expression of g_e and Eq. (6) for the relationship between ξ_e and g_e]. In addition, since $d_g < d_0$, one can expect a uniform monomer concentration c within all the blobs; therefore, the concentration c appearing in the expression for ξ_e [see Eq. (11)] can be expressed as

$$c \sim \frac{N\sigma_g}{d_g}. \tag{17}$$

Under all these conditions, for semidilute PE brush bilayers (BBLs) in the intermediate IP regime (i.e., $d_g < d_0$) we can obtain from Eq. (16)

$$\delta \sim \xi_e^{4/3}\left(\frac{N}{g_e}\right)^{2/3} d_g^{-1/3} \sim a(a^2\sigma_g)^{-1/3} N^{1/3} (uf^2)^{\frac{1-\nu}{6-3\nu}}. \tag{18}$$

Equation (18) follows directly from the expressions provided in Ref. [71].

D. Scaling laws for polyelectrolyte brush bilayers in weakly interpenetration regime

For this case $d_0 < d_g < 2d_0$, where either Eq. (13) or Eq. (14) defines d_0. Obviously, for this case all the Kuhn segments (or monomers) *are not located in the interpenetrated region*. Similar to our previous study [70], here too we consider that N_1 number of monomers (or Kuhn segments) are outside the interpenetration region while $N - N_1$ number of monomers are inside the interpenetration region. Accordingly, we replace a by ξ_e and N by $(N - N_1)/g_e$ in Eq. (16). Furthermore, c appearing in the expression of ξ_e would be

$$c_\delta \sim \frac{(N - N_1)\sigma_g}{\delta}. \tag{19}$$

Also, we use Eq. (6) to relate ξ_e and g_e. Under these conditions, we may finally obtain from Eq. (16)

$$\delta \sim a\left(a^{1/2} d_g^{-1/2}\right)(a^2\sigma_g)^{-1/2} N^{1/2}\left(1 - \frac{N_1}{N}\right)^{1/2} (uf^2)^{\frac{1-\nu}{4-2\nu}}. \tag{20}$$

The next important step is to express N_1/N in terms of $x = d_g/d_0$. We assume that the segment of the PE molecule that is outside the IP regime will definitely form brushes. Let us consider the height of this brush segment as d_1. Therefore, following Desai *et al.* [70]:

$$d_1 \sim d_g - d_0. \tag{21}$$

In the case $\sigma_g^* < \sigma_g < \sigma_{osm}$, i.e., the brushes form Pincus brushes, we can write [from Eq. (13)]

$$d_{1,PB} \sim K_1 N_1^{\frac{2-\nu}{\nu}}, \quad d_{0,PB} \sim K_1 N^{\frac{2-\nu}{\nu}}. \tag{22}$$

Using Eq. (22) in Eq. (21), we can write that, for Pincus brushes,

$$x_{PB} = \left(\frac{d_g}{d_0}\right)_{PB} \sim 1 + \left(\frac{N_1}{N}\right)^{\frac{2-\nu}{\nu}}. \tag{23}$$

On the other hand, when the brushes form osmotic brushes (i.e., when $\sigma_g > \sigma_{osm}$), we can have [using Eq. (14)]

$$d_{1,OB} \sim K_2 N_1, \quad d_{0,OB} \sim K_2 N. \tag{24}$$

Therefore, using Eq. (24) in Eq. (21), we can write

$$x_{OB} = \left(\frac{d_g}{d_0}\right)_{OB} \sim 1 + \frac{N_1}{N}. \tag{25}$$

Consequently, using either Eq. (23) or Eq. (25) in Eq. (20), we may write

$$\delta_{PB} \sim a(a^{1/2}d_g^{-1/2})(a^2\sigma_g)^{-1/2}N^{1/2} \times [1-(x-1)^{\frac{\nu}{2-\nu}}]^{1/2}(uf^2)^{\frac{1-\nu}{4-2\nu}}, \quad (26)$$

$$\delta_{\rm OB} \sim a\left(a^{1/2}d_g^{-1/2}\right)(a^2\sigma_g)^{-1/2}N^{1/2}(2-x)^{1/2}(uf^2)^{\frac{1-\nu}{4-2\nu}}. \quad (27)$$

Here δ_{PB} represents the IP length for PE brushes in weak IP regime with the brush segment (outside the IP zone) being described as a Pincus brush. On the other hand, $\delta_{\rm OB}$ represents the IP length for PE brushes in weak IP regime with the brush segment (outside the IP zone) being described as an osmotic brush.

It is useful to reiterate here the strategy of obtaining the scaling laws in Eqs. (26) and (27). We start from Eq. (16). We consider the changes to this equation due to (a) the brush being in the semidilute regime, (b) a part of the polymer molecule that is outside the interpenetration region will form a brush (either Pincus or osmotic, based on the grafting density), and (c) part of the polymer molecule that is inside the IP zone can be considered to be divided into blobs, with each blob having a uniform monomer density. The appropriate mathematical representations of these considerations (summarized in the first part of this section) along with the use of Eq. (6) eventually ensure that we obtain Eq. (26) or Eq. (27) from Eq. (16).

III. MOLECULAR DYNAMICS SIMULATIONS

We employ the Large-scale Atomic/Molecular Massively Parallel Simulator (LAMMPS) software package [80] to carry out the MD simulations for studying a system of $2M = 72$ end-grafted PE chains, with $M = 36$ chains grafted on each of the two opposing walls. We consider a grafting density of $\sigma_g = 0.2/\sigma_{LJ}^2$. Each PE chain is represented as a bead-spring system of N beads, with each bead having a radius of σ_{LJ} and a charge of $-1e$ (where e is the electronic charge). Out of these N beads, one bead is grafted to the wall. This particular bead remains stationary and is assumed to be devoid of any charge. Therefore, there are $2 \times M \times (N-1)$ charged polymer beads. Next, we add in the system $2 \times M \times (N-1)$ beads, each containing a charge of $+e$, in order to explicitly model the counterions and to ensure a net charge neutrality of the system. The equation of motion of bead i, where i represents all the beads of the PE chain (except the bead that is fixed at the grafting surface) as well as the beads representing the counterions, can be expressed as [70]

$$m\frac{d^2\vec{r}_i}{dt^2} = -\vec{\nabla}_i U_{\rm total} - \gamma_D m\frac{d\vec{r}_i}{dt} + \vec{\Gamma}_i(t), \quad (28)$$

where m is the mass of bead i (we assume assume identical mass for all the beads, regardless of whether they represent monomers or counterions), $\vec{r}_i$ is the position vector of bead i, $-\vec{\nabla}_i U_{\rm total}$ is the total force acting on bead i, γ_D is the damping coefficient, and $\vec{\Gamma}_i(t)$ is the time-dependent random force that bead i experiences. $U_{\rm total}$ appearing in Eq. (28) is expressed differently for the monomers and the counterions. For the monomers we call it $U_{{\rm total},m}$, while for the counterions we call it $U_{{\rm total},c}$, with

$$U_{{\rm total},m} = U_{LJ,{\rm bead},ij} + U_{LJ,{\rm wall},i} + U_{{\rm FENE},i} + U_{{\rm Coul},ij}, \quad (29)$$

$$U_{{\rm total},c} = U_{LJ,{\rm bead},ij} + U_{LJ,{\rm wall},i} + U_{{\rm Coul},ij}. \quad (30)$$

In the above equations, $U_{LJ,{\rm bead},ij}$ represents the shifted Lennard–Jones (LJ) interaction potential between beads i and j ($j \neq i$), $U_{LJ,{\rm wall},i}$ represents the shifted LJ interaction potential between bead i and the wall, $U_{{\rm Coul},ij}$ represents the Coulombic interaction potential between beads i and j ($j \neq i$), and $U_{{\rm FENE},i}$ represents the finite extensible nonlinear elastic (FENE) bond potential between bead i and j (where $j = i+1, i-1$ and beads i and j represent only the beads of the PE chain). We refer to Desai *et al.* [70] for the detailed expressions for $U_{LJ,{\rm bead},ij}$, $U_{LJ,{\rm wall},i}$, and $U_{{\rm FENE},i}$ as well as the values of the different parameters defining these potentials. Finally, we can express $U_{{\rm Coul},ij}$ as

$$U_{{\rm Coul},ij} = k_B T \ell_B \frac{q_i q_j}{r_{ij}}, \quad (31)$$

where q_i and q_j are charges on beads i and j, r_{ij} is the distance between beads i and j, and $\ell_B = \sigma_{LJ}$ is the Bjerrum length.

We simulate a system on $N = 20, 40, 75$ PE chains. The simulations are carried out in an NVT ensemble using a Langevin thermostat. The electrostatic interactions in the simulations are calculated by using particle-particle particle-mesh (PPPM) method [81] for slab geometry [82], with periodic boundary condition in x plane and y plane but nonperiodic in the z plane. All the simulations are carried out using a time step of $0.006\tau_{LJ}$ [where $\tau_{LJ} = \sigma_{LJ}(m/\epsilon_{LJ})^{1/2}$ with ϵ_{LJ} being the characteristic LJ energy scale]. The grafted PE chains along with the counterions, *in absence of any interpenetration*, are first equilibrated for 5×10^6 time steps. This equilibrated system, therefore, consists of PE molecules (grafted to two opposing plates in a manner such that $d_g \gg 2d_0$) and oppositely charged counterions. Subsequently, we bring the two grafting surfaces closer to each other such that $d_0 < d_g < 2d_0$. Once the opposing surfaces are at the desired value of d_g/d_0, we equilibrate the PE chains by simultaneously using the "NVE/LIMIT" command and the Langevin thermostat for 1000–10000 time steps. This procedure ensures that the displacements in the simulations are not unphysically large. In the next step, we equilibrate the system for another 3×10^6 time steps, followed by a production run of 2×10^6 time steps. During this production run, data are collected after every 1000 time steps. Since the typical relaxation time of the PE brush system that we study is merely a few hundred LJ time units [83], we believe that our results represent perfectly equilibrated interpenetrated PE-brush-counterion system. To be even more certain, we ourselves calculated the autocorrelation function and the corresponding relaxation time for our system. We found very similar relaxation times of merely a few hundred LJ time units as noted in the literature [83] and therefore we are convinced that our results represent an equilibrium behavior. In Figs. 1 and 2, we show the MD simulation snapshots for the PE BBLs for the different degree of interpenetration for $N = 40$ and $N = 75$, respectively. These figures, whose sizes

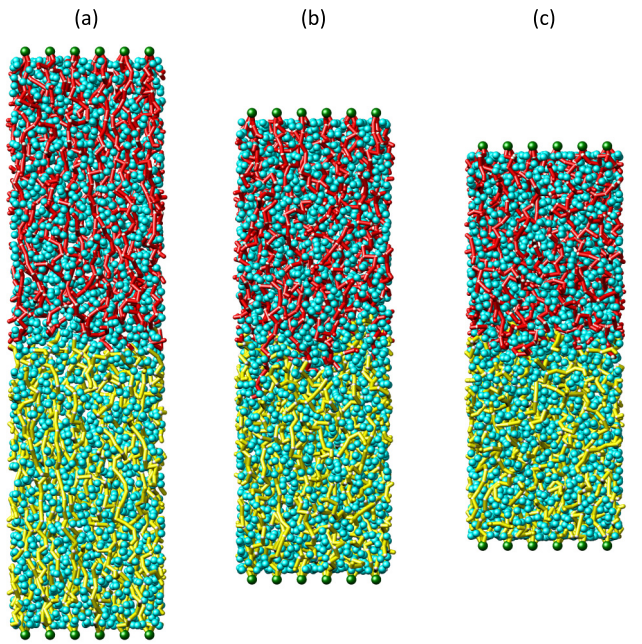

FIG. 1. Snapshots of the interpenetrating PE brushes for $N = 40$ for (a) $d_g/d_0 = 1.75$, (b) $d_g/d_0 = 1.4$ and (c) $d_g/d_0 = 1.2$. The PE brushes are shown with yellow and red, while the counterions are shown with blue.

represent the plate gap d_g, are the representative snapshots that are later used to quantify the interpenetration behavior through a more detailed quantification of the variation of the IP length δ (Fig. 3) as well as the monomer concentration distribution (Fig. 4).

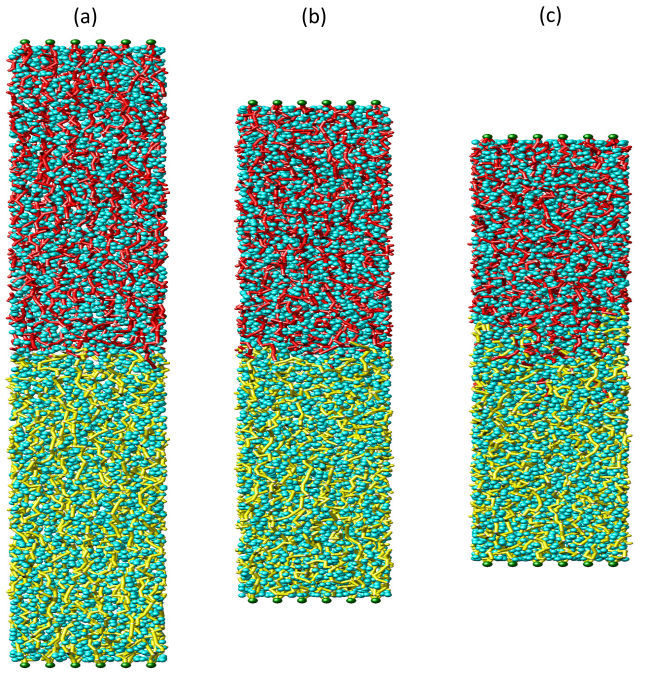

FIG. 2. Snapshots of the interpenetrating PE brushes for $N = 75$ for (a) $d_g/d_0 = 1.75$, (b) $d_g/d_0 = 1.4$ and (c) $d_g/d_0 = 1.2$. The PE brushes are shown with yellow and red, while the counterions are shown with blue.

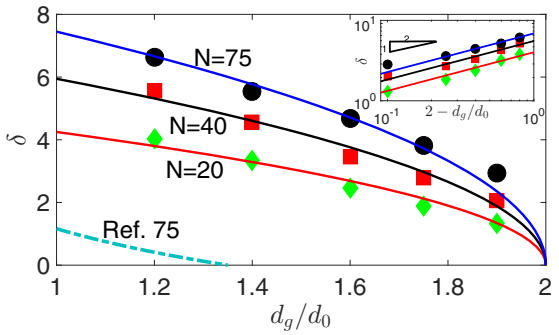

FIG. 3. Variation of interpenetration length δ (in units of σ_{LJ}) with d_g/d_0 for different N for polymer (P) and polyelectrolyte (PE) brushes. The markers are the MD results, while the continuous lines are the scaling predictions of the form $\delta = \delta_{\rm OB} = C_1 N^{1/2}(2 - d_g/d_0)^{1/2}$ [this form of equation is obtained from Eq. (27)]. The fit is obtained for nearly constant values of C_1 for all the three values of N [$(C_1)_{N=75} = 0.86$, $(C_1)_{N=40} = 0.94$, $(C_1)_{N=20} = 0.95$], establishing the rigour of the scaling law. In the inset of the figure, we provide this comparison between the MD and the scaling predictions on a log-log scale. Clear 1/2-power dependence of δ on $2 - d_g/d_0$ is evident. Also in the main figure, we provide the δ variation obtained from the phenomenological scaling prediction of Ref. [75], which states $\delta \sim (d_g/d_0)^{-3/2}[1 - (d_g/1.35d_0)^2]$ (i.e., they assume that there is no IP for $d_g/d_0 > 1.35$).

IV. INTERPENETRATION LENGTH δ OF POLYELECTROLYTE BRUSH BILAYERS

We use the MD simulations to compute the IP length δ [44] for the PE BBLs for different values of d_g/d_0 in the weak IP regime (i.e., $d_0 < d_g < 2d_0$) and different N. For the present case, we use a grafting density of $\sigma_g = 0.2/\sigma_{\rm LJ}^2$ (where $\sigma_{\rm LJ} \sim 1$ nm is the LJ length scale), $f = 1$, and $a = \sigma_{\rm LJ}$. Therefore, $\sigma_g \gg \sigma_{\rm osm}$ [see Eq. (12) for $\sigma_{\rm osm}$] for all the values of N that we consider, ensuring that the brushes are always in the osmotic regime. Please note that here by "brushes in the osmotic regime," we imply the PE segments that are present outside the IP regime and are assumed to form brushes (please see Sec. II D for more details). Therefore, the corresponding the scaling prediction for the IP length $\delta_{\rm OB}$ is provided by Eq. (27)—we can consider this scaling expression of the form $\delta_{\rm OB} = C_1 N^{1/2}(2 - x)^{1/2}$. Figure 3 provides the comparison between the MD simulation result and the scaling prediction for δ. We witness an excellent match for most of the values of d_g/d_0 and N, except for $d_g/d_0 = 1.9$ for $N = 75$. In the inset of the figure, we provide the log-log plot showing the clear 1/2-power dependence of δ on $2 - d_g/d_0$. To the best of our knowledge there has been only one study that probes the weakly interpenetrated PE BBL by simultaneous use of MD simulation and scaling prediction [75]—however, the scaling theory that has been derived in this paper to match the MD predictions is a "phenomenological" one without being derived from the rigorous free-energy consideration. On the contrary, the theory derived here strictly obeys the free-energy consideration and the corresponding match with respect to the MD simulation results, demonstrating the dependence of δ on the extent of interpenetration (IP) and the value of N, is extremely accurate.

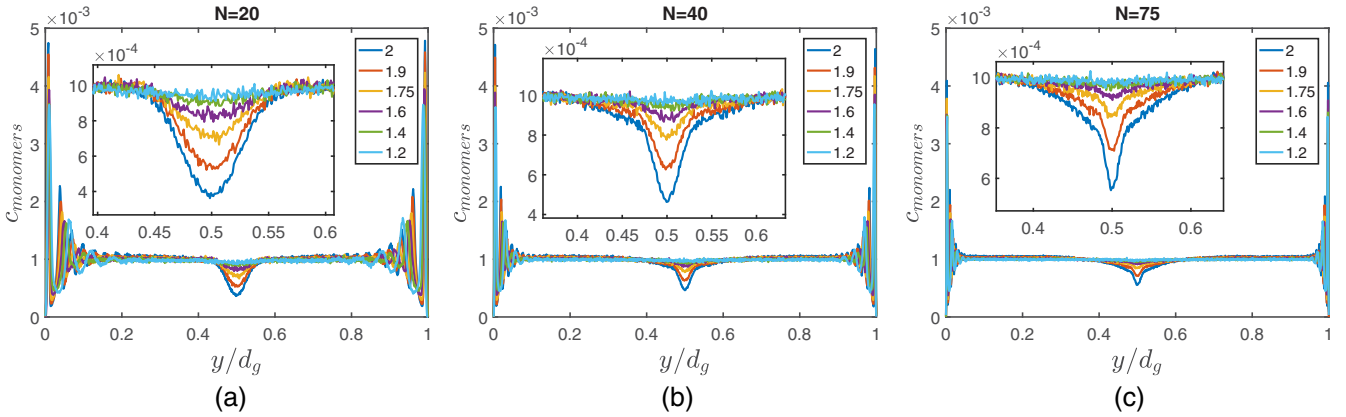

FIG. 4. Monomer concentration distribution (c_{monomer}) for different d_g/d_0 values (see the legend) for (a) $N = 20$, (b) $N = 40$, and (c) $N = 75$. c_{monomer} is normalized, i.e., $\int_0^{d_g} c_{\text{monomer}} dy = 1$. In the inset of each figure, we magnify the monomer concentration distribution near the channel centerline.

There is another extremely important connotation of Fig. 3, with respect to the existing studies of weakly interpenetrating PE BBLs [71,75]. One of these studies, for example, predicts absolutely no interpenetration (i.e., $\delta \to 0$) for weak IP regime [71]. On the other hand, Kumar and Siedel [75] predicts interpenetration only for very relatively small values of d_g, i.e., for $d_g/d_0 \leqslant 1.35$. In Fig. 3, we also provide this scaling prediction of Ref. [75]. Both our MD simulations as well as scaling predictions strongly contradict these findings and establish that there will be a finite δ as long as $d_g < 2d_0$.

V. MONOMER AND COUNTERION CONCENTRATION DISTRIBUTION

Figure 4 shows the monomer distribution with y for different values of the degree of interpenetration (d_g/d_0) and N. For any given N, smaller interpenetration (or larger d_g/d_0) leads to a more "single-plate-like" monomer distribution. Consequently, the monomer density decreases away from the grafting surface. For any given N, increase in the degree of interpenetration (or decrease in d_g/d_0) leads to the onset of overlap of the PE brushes from the opposing surfaces. Therefore, monomer concentration decreases much more weakly away from the grafting surface, eventually ensuring virtually uniform monomer distribution across the channel for a large degree of interpenetration ($d_g/d_0 \sim 1.2$). Larger N implies a larger number of monomers. Therefore, an increase in N implies that for any given degree of interpenetration (or a given d_g/d_0), we find a larger value of the monomer concentration at a given distance from the wall, regardless of the extent of lowering of the monomer concentration away from the grafting surface. Figure 4 demonstrating the existence of finite monomer concentration near the channel centerline (i.e., the IP zone) even for much larger d_g/d_0 (i.e., d_g/d_0 close to 2) is perfectly commensurate with the prediction of a finite δ (see Fig. 3) for such d_g/d_0 values.

Figure 5 shows the counterion concentration distribution for different d_g/d_0 and N. The counterion concentration distribution, at least qualitatively, obeys the monomer concentration distribution for the major part of the nanochannel. Therefore, the counterion concentration decreases near the channel centerline (similar to what happens with the monomer concentration distribution; see Fig. 4) for all values of N for relatively weaker degree of IP (i.e., larger values of d_g/d_0).

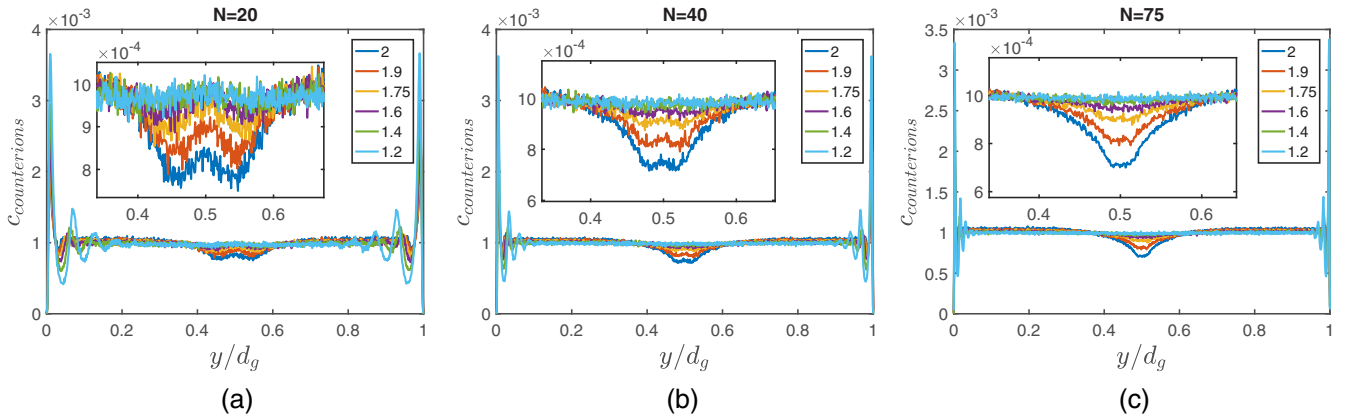

FIG. 5. Counterion concentration distribution ($c_{counterion}$) for different d_g/d_0 values (see the legend) for (a) $N = 20$, (b) $N = 40$, and (c) $N = 75$. $c_{counterion}$ is normalized, i.e., $\int_0^{d_g} c_{counterion} dy = 1$. In the inset of each figure, we magnify the counterion concentration distribution near the channel centerline.

Similarly for all N, for a larger degree of IP (or smaller values of d_g/d_0), we witness a more or less uniform counterion concentration distribution (similar to the case of monomer distribution; see Fig. 4) across the channel cross section. This is perfectly commensurate with the idea of osmotic PE brushes, where the counterions remain tightly bound to the brushes. Of course, there is a quantitative variation between the monomer and counterion concentration distributions, particularly near the channel centerline (i.e., the interpenetration zone)—at that location the monomer concentration decreases steeply while the corresponding counterion concentration shows a much flatter decrease. For example, for a given N, the monomer distribution, for weak IP, demonstrates a much steeper decay away from the channel walls, while the counterion concentration distribution shows a much flatter decay away from the wall.

VI. CONCLUSIONS

Our analyses, involving scaling calculations and MD simulations, establish that, for PE BBLs, finite interpenetration is likely as long as $d_g < 2d_0$, while the existing theories have proposed that such an interpenetration will occur only for much smaller values of d_g (i.e., when d_g is smaller than or slightly larger than d_0). Our conclusions, unlike these studies, are based on a combination of extensive MD simulations and scaling calculations that involve rigorous free-energy considerations. Furthermore, our results provide a unique combined picture of the monomer and counterion concentration distributions. These distributions, obeying the condition of osmotic brushes, follow each other closely qualitatively for the major part of the channel. Of course, near the channel centerline (i.e., the location of the interpenetration), these distributions quantitatively deviate from each other—the monomer distribution demonstrates a much steeper decay as compared with the counterions. However, they quantitatively deviate from each other at the channel centerline. We believe that these results, like the results of our previous paper on weakly interpenetrated *polymer BBLs*, will provide a quantitative basis for probing the physics of the weakly interpenetrated PE BBLs.

[1] K. Binder, A. Milchev, and J. Baschnagel, Annu. Rev. Mater. Sci. **26**, 107 (1996).
[2] R. R. Netz and D. Andelman, Phys. Rep. **380**, 1 (2003).
[3] D. Marsh, R. Bartucci, and L. Sportelli, Biochim. Biophys. Acta, Biomembr. **1615**, 33 (2003).
[4] S. Minko, J. Macromol. Sci., Polym. Rev. **46**, 397 (2006).
[5] P. Jain, G. L. Baker, and M. L. Bruening, Annu. Rev. Anal. Chem. **2**, 387 (2009).
[6] S. Das, M. Banik, G. Chen, S. Sinha, and R. Mukherjee, Soft Matter **11**, 8550 (2015).
[7] M. Ali, B. Yameen, R. Neumann, W. Ensinger, W. Knoll, and O. Azzaroni, J. Am. Chem. Soc. **130**, 16351 (2008).
[8] S. Umeharaa, M. Karhaneka, R. W. Davis, and N. Pourmanda, Proc. Natl. Acad. Sci. USA **106**, 4611 (2009).
[9] M. Ali, B. Yameen, J. Cervera, P. Ramirez, R. Neumann, W. Ensinger, W. Knoll, and O. Azzaroni, J. Am. Chem. Soc. **132**, 8338 (2010).
[10] G. Chen and S. Das, J. Appl. Phys. **117**, 185304 (2015).
[11] G. Chen and S. Das, J. Phys. Chem. B **121**, 3130 (2017).
[12] H. Otsuka, Y. Nagasaki, and K. Kataoka, Adv. Drug Delivery Rev. **55**, 403 (2003).
[13] H. ShamsiJazeyi, C. A. Miller, M. S. Wong, J. M. Tour, and R. Verduzco, J. Appl. Polym. Sci. **131**, 40576 (2014).
[14] M. Ballauff and O. Borisov, Curr. Opin. Colloid Interface Sci. **11**, 316 (2006).
[15] S. Alexander, J. Phys. (Paris) **38**, 977 (1977).
[16] P. G. de Gennes, J. Phys. (Paris) **37**, 1443 (1976).
[17] P.-G. de Gennes, Macromolecules (Washington, DC, U. S.) **13**, 1069 (1980).
[18] S. T. Milner, T. A. Witten, and M. E. Cates, Europhys. Lett. **5**, 413 (1988).
[19] S. T. Milner, T. A. Witten, and M. E. Cates, Macromolecules (Washington, DC, U. S.) **21**, 2610 (1988).
[20] E. B. Zhulina, V. A. Priamitsyn, and O. V. Borisov, Polym. Sci. U.S.S.R. **31**, 205 (1989).
[21] S. T. Milner, Science **251**, 905 (1991).
[22] P. Pincus, Macromolecules (Washington, DC, U. S.) **24**, 2912 (1991).
[23] S. Misra, S. Varanasi, and P. P. Varanasi, Macromolecules (Washington, DC, U. S.) **22**, 4173 (1989).
[24] S. Misra, M. Tirrell, and W. Mattice, Macromolecules (Washington, DC, U. S.) **29**, 6056 (1996).
[25] R. S. Ross and P. Pincus, Macromolecules (Washington, DC, U. S.) **25**, 2177 (1992).
[26] E. B. Zhulina and O. V. Borisov, J. Chem. Phys. **107**, 5952 (1997).
[27] E. B. Zhulina and O. V. Borisov, Langmuir **27**, 10615 (2011).
[28] E. B. Zhulina and M. Rubinstein, Soft Matter **8**, 9376 (2012).
[29] G. Chen and S. Das, J. Phys. Chem. B **120**, 6848 (2016).
[30] T. Kreer, Soft Matter **12**, 3479 (2016).
[31] J. Klein, D. Perahia, and S. Warburg, Nature (London) **352**, 143 (1991).
[32] H. J. Taunton, C. Toprakcioglu, L. J. Fetters, and J. Klein, Nature (London) **332**, 712 (1988).
[33] J. Klein, Colloids Surf., A **86**, 63 (1994).
[34] R. Tadmor, J. Janik, J. Klein, and L. J. Fetters, Phys. Rev. Lett. **91**, 115503 (2003).
[35] S. de Beer, G. D. Kenmoé, and M. H. Müser, Friction **3**, 148 (2015).
[36] S. de Beer and M. H. Müser, Macromolecules (Washington, DC, U. S.) **47**, 7666 (2014).
[37] S. de Beer, E. Kutnyanszky, P. M. Schön, G. J. Vancso, and M. H. Müser, Nat. Commun. **5**, 3781 (2014).
[38] J.-M. Y. Carrillo, D. Russano, and A. V. Dobrynin, Langmuir **27**, 14599 (2011).
[39] J.-M. Y. Carrillo, W. M. Brown, and A. V. Dobrynin, Macromolecules (Washington, DC, U. S.) **45**, 8880 (2012).
[40] S. M. Balko, T. Kreer, P. J. Costanzo, T. E. Patten, A. Johner, T. L. Kuhl, and C. M. Marques, PLoS One **8**, e58392 (2013).
[41] J. Klein, Science **323**, 47 (2009).

[42] T. Moro, Y. Takatori, K. Ishihara, T. Konno, Y. Takigawa, T. Matsush, U. Chung, K. Nakamura, and H. Kawaguchi, Nat. Mater. **3**, 829 (2004).
[43] T. Kreer, M. H. Müser, K. Binder, and J. Klein, Langmuir **17**, 7804 (2001).
[44] L. Spirin, A. Galuschko, T. Kreer, A. Johner, J. Baschnagel, and K. Binder, Eur. Phys. J. E: Soft Matter Biol. Phys. **33**, 307 (2010).
[45] A. Galuschko, L. Spirin, T. Kreer, A. Johner, C. Pastorino, J. P. Wittmer, and J. Baschnagel, Langmuir **26**, 6418 (2010).
[46] G. S. Grest, Lect. Notes Phys. **138**, 149 (1999).
[47] M. Murat and G. S. Grest, Phys. Rev. Lett. **63**, 1074 (1989).
[48] T. Kreer, K. Binder, and M. H. Müser, Langmuir **19**, 7551 (2003).
[49] L. Chen, H. Merlitz, S.-Z. He, C.-X. Wu, and J.-U. Sommer, Macromolecules (Washington, DC, U. S.) **44**, 3109 (2011).
[50] L. Spirin, A. Galuschko, and T. Kreer, Macromolecules (Washington, DC, U. S.) **44**, 9399 (2011).
[51] T. Kreer and S. M. Balko, ACS Macro Lett. **2**, 944 (2013).
[52] V. M. Amoskov, T. M. Birshtein, and V. A. Pryamitsyn, Macromolecules (Washington, DC, U. S.) **31**, 3720 (1998).
[53] A. Chakrabarti, P. Nelson, and R. Toral, J. Chem. Phys. **100**, 748 (1994).
[54] A. Wynveen and C. N. Likos, Phys. Rev. E **80**, 010801(R) (2009).
[55] T. A. Witten, L. Leibler, and P. A. Pincus, Macromolecules (Washington, DC, U. S.) **23**, 824 (1990).
[56] H. Ohshima, Adv. Colloid Interface Sci. **226**, 2 (2015).
[57] H. Ohshima, Colloid Polym. Sci. **292**, 431 (2014).
[58] G. S. Grest, Phys. Rev. Lett. **76**, 4979 (1996).
[59] I. G. Elliott, T. L. Kuhl, and R. Faller, J. Phys. Chem. B **117**, 4134 (2013).
[60] M. K. Singh, P. Ilg, R. M. Espinosa-Marzal, M. Kröger, and N. D. Spencer, Langmuir **31**, 4798 (2015).
[61] D. Russano, J-M. Y. Carrillo, and A. V. Dobrynin, Langmuir **27**, 11044 (2011).
[62] A. G. Goicochea, E. Mayoral, J. Klapp, and C. Pastorino, Soft Matter **10**, 166 (2014).
[63] A. Erbas and J. Paturej, Soft Matter **11**, 3139 (2015).
[64] P. A. Schorr, T. C. B. Kwan, S. M. Kilbey II, E. S. G. Shaqfey, and M. Tirrell, Macromolecules (Washington, DC, U. S.) **36**, 389 (2003).
[65] E. Eiser and J. Klein, Macromolecules (Washington, DC, U. S.) **40**, 8455 (2007).
[66] L. Tsarkova, X. Zhang, N. Hadjichristidis, and J. Klein, Macromolecules (Washington, DC, U. S.) **40**, 2539 (2007).
[67] O. Tairy, N. Kampf, M. J. Driver, S. P. Armes, and J. Klein, Macromolecules (Washington, DC, U. S.) **48**, 140 (2015).
[68] R. Krishnamoorti and E. P. Giannelis, Langmuir **17**, 1448 (2001).
[69] C. M. Wijmans and B. Smit, Macromolecules (Washington, DC, U. S.) **35**, 7138 (2002).
[70] P. R. Desai, S. Sinha, and S. Das, Soft Matter **13**, 4159 (2017).
[71] E. B. Zhulina and M. Rubinstein, Macromolecules (Washington, DC, U. S.) **47**, 5825 (2014).
[72] J. B. Sokoloff, J. Chem. Phys. **129**, 014901 (2008).
[73] M. W. Matsen, Eur. Phys. J. E: Soft Matter Biol. Phys. **34**, 45 (2011).
[74] L. Spirin and T. Kreer, ACS Macro Lett. **2**, 63 (2013).
[75] N. A. Kumar and C. Seidel, Phys. Rev. E **76**, 020801(R) (2007).
[76] M. Balastre, F. Li, P. Schorr, J. Yang, J. W. Mays, and M. V. Tirrell, Macromolecules (Washington, DC, U. S.) **35**, 9480 (2002).
[77] F. Goujon, A. Ghoufi, P. Malfreyt, and D. Tildesley, Soft Matter **9**, 2966 (2013).
[78] M. Chen, W. H. Briscoe, S. P. Armes, and J. Klein, Science **323**, 1698 (2009).
[79] H. Ahrens, S. Förster, C. A. Helm, N. A. Kumar, A. Naji, R. R. Netz, and C. Seidel, J. Phys. Chem. B **108**, 16870 (2004).
[80] S. Plimpton, J. Comput. Phys. **117**, 1 (1995).
[81] R. W. Hockney and J. W. Eastwood, *Computer Simulation Using Particles* (Adam Hilger, New York, 1989).
[82] C. Yeh and M. L. Berkowitz, J. Chem. Phys. **111**, 3155 (1999).
[83] C. Siedel, Macromolecules (Washington, DC, U. S.) **36**, 2536 (2003).